

Flow around fishlike shapes studied using multiparticle collision dynamics

Daniel A. P. Reid,¹ H. Hildenbrandt,¹ J. T. Padding,² and C. K. Hemelrijk^{1,*}

¹*Theoretical Biology, Rijksuniversiteit Groningen, Kerklaan 30, Haren, The Netherlands*

²*Computational Biophysics, University of Twente, Enschede, The Netherlands*

(Received 4 July 2008; published 14 April 2009)

Empirical measurements of hydrodynamics of swimming fish are very difficult. Therefore, modeling studies may be of great benefit. Here, we investigate the suitability for such a study of a recently developed mesoscale method, namely, multiparticle collision dynamics. As a first step, we confine ourselves to investigations at intermediate Reynolds numbers of objects that are stiff. Due to the lack of empirical data on the hydrodynamics of stiff fishlike shapes we use a previously published numerical simulation of the shapes of a fish and a tadpole for comparison. Because the shape of a tadpole resembles that of a circle with an attached splitter plate, we exploit the knowledge on hydrodynamic consequences of such an attachment to test the model further and study the effects of splitter plates for objects of several shapes at several Reynolds numbers. Further, we measure the angles of separation of flow around a circular cylinder and make small adjustments to the boundary condition and the method to drive the flow. Our results correspond with empirical data and with results from other models.

DOI: [10.1103/PhysRevE.79.046313](https://doi.org/10.1103/PhysRevE.79.046313)

PACS number(s): 47.63.-b, 47.11.-j

I. INTRODUCTION

Mesoscale models of fluid dynamics have been used to study many phenomena in fields such as physics and biochemistry. Examples include flow around cylinders [1], molecular diffusion [2], polymers in flow [3], and the formation of micelles [4]. They have also been applied to study biological systems, mainly at the cellular level, for example red blood cells in flow [5]. In the present paper we test whether a mesoscale model of hydrodynamics, namely multiparticle collision dynamics [6,7], is suitable to study stiff fishlike shapes in flow. This is part of a long-term project to investigate the hydrodynamics of actively swimming fish, both alone and in a group. We prefer a mesoscale model over the numerical methods derived from the Navier-Stokes equations of flow used for similar problems [8,9] because it allows us to study the hydrodynamics of any shape without needing to adapt a coordinate grid to it [10] or add additional assumptions, such as to impose vorticity [8] or to use a special boundary condition for edges such as a tail fin [9]. Further, since it is an off-grid method, it is one of the most suitable mesoscale methods to extend with objects that deform, such as an undulating fish.

The multiparticle collision dynamics model was introduced by Malevanets and Kapral [6] and has since been used to investigate a variety of microscale hydrodynamic systems [3,11–13]. The model consists of a fluid of particles which move and collide, whereby the collisions conserve both mass and momentum. At the macroscale the system exhibits behavior that is consistent with the Navier-Stokes laws of hydrodynamics. Expressions for the viscosity and several transport coefficients have been derived [14], showing that the model is correct as regards both short- and long-range hydrodynamics.

Although fish swim at high Reynolds numbers of 10^3 up to 10^5 [15], in the present study we confine ourselves to

intermediate Reynolds numbers (i.e., Re 10–110) which are relevant for fish larvae [16]. We use these lower Reynolds numbers for two reasons. First, it reduces computational effort, which scales quadratically with the Reynolds number. Second, the comparability to earlier studies at the same Reynolds number of hydrodynamics of a circle and square [17,18].

In this paper we confine ourselves to the study of stiff shapes, with the aim to later extend the model to deformable ones. Because empirical data on hydrodynamic traits of stiff fish are lacking we use other data, namely, previously published results of a numerical simulation of a fish and a tadpole [10,19]. Apart from this comparison we note that the shape of a tadpole resembles that of a circle with an attached splitter plate. This resemblance we exploit because much is known about the hydrodynamic effects of splitter plates [20]. Therefore we examine flow around, and drag of a circle with and without a splitter plate attached to it. We do so for a series of different Re numbers and object shapes. We further verify our implementation for a circular cylinder with a new measurement, namely, of the separation angle of flow. Our results confirm the suitability of the model for the study of the hydrodynamics of fishlike shapes.

II. METHODS

A. System overview

We investigate the hydrodynamics of objects held in place in a channel. Although the model has been shown to perform well in three dimensions [21], we use two-dimensional simulations to reduce computational effort. A schematic overview of the system is shown in Fig. 1. The channel has width W and length L . We set these to be the same as those used by Lamura and Gompper [17,18], against whose work we compare our results. The width and length are both functions of the cross section D of the object, with $W=8D$ and $L=50D$. This results in a blockage ratio $B=D/W$ of 0.125 [17]. The channel has solid walls at the top and bottom, and is periodic

*c.k.hemelrijk@rug.nl

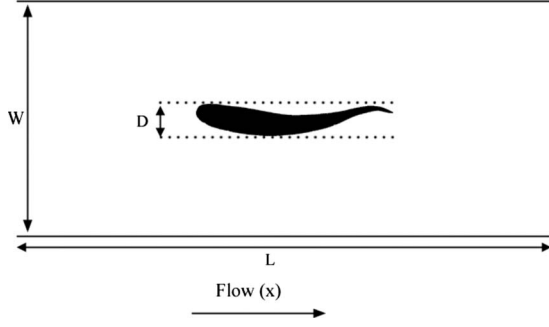


FIG. 1. The simulation setup. W is the width of the channel, L is its length (not to scale), and D is the object diameter, measured along the width axis.

in the x direction. All objects are represented as polygons so that they may have any shape. We use a relatively wide system so that the wake of the object will die out before it encounters the object again. Flow goes from left to right. We calculate the Reynolds number as

$$\text{Re} = \frac{\rho v_x D}{\mu}, \quad (1)$$

where ρ is the fluid density, v_x is the flow speed along the channel center far away from the object, and μ is the dynamic viscosity which consists of two components [Eq. (4), see below].

B. Multiparticle collision dynamics

The system consists of a two-dimensional homogeneous space containing N identical particles of mass m . The positions \mathbf{x}_i and velocities \mathbf{v}_i of the particles are two-dimensional vectors of continuous variables. Every time step Δt the particles first move and then collide. Moving leads to new positions \mathbf{x}_i according to Eq. (2),

$$\mathbf{x}_i(t + \Delta t) = \mathbf{x}_i(t) + \mathbf{v}_i(t)\Delta t. \quad (2)$$

To simulate collisions, a square lattice with mesh size a_0 is used to partition the system. In each lattice cell, all particles simultaneously collide with each other, changing their velocities according to

$$\mathbf{v}_i = \bar{\mathbf{v}} + \omega(\mathbf{v}_i - \bar{\mathbf{v}}). \quad (3)$$

Here $\bar{\mathbf{v}}$ is the mean velocity of the particles in the grid cell and ω is a stochastic rotation matrix that rotates the velocities by either $+\alpha$ or $-\alpha$ (where α is a fixed system parameter), with equal probability. It is the same for all particles within a cell. The rotation procedure can thus be viewed as a coarse-graining of particle collisions over space and time. We set α to $\frac{\pi}{2}$ for three reasons. First, because it is the value used in the studies to which we compare our results [17,18]. Second, because Allahyarov and Gompper [21] showed that the kinematic viscosity is lowest for this value of α , thus maximizing the Reynolds number. Third, because rotation by $\frac{\pi}{2}$ is computationally very fast.

An overview of parameter settings is shown in Table I. From these parameters we derive the mean-free path, which

TABLE I. Parameter values used.

Parameter name	Symbol	Value used
Temperature	$k_B T$	1.0
Lattice cell size	a_0	1.0
Collision rotation angle	α	$\frac{\pi}{2}$
Particle mass	m	1.0
Particles per cell (average)	ρ	10
Time step length	Δt	1.0

is the mean distance traveled by a particle before it collides. This path length is given by the expression $l = \Delta t \sqrt{k_B T / m}$, where k_B is the Boltzmann constant, and T is the temperature of the system. If the system temperature and thus the mean-free path are low, and $l < a_0$, the same particles will often collide with each other on consecutive time steps, which breaks Galilean invariance. To solve this problem we follow the solution proposed by Ihle and Kroll [22] and displace the lattice every time step by a vector with x and y components which are randomly selected from the interval $[0, a_0]$.

An important advantage of this method is that its simplified dynamics has allowed the analytic calculation of several transport properties [14]. The most important one for this study is the viscosity μ , which consists of two components,

$$\mu = \mu_{\text{kin}} + \mu_{\text{coll}}, \quad (4)$$

where μ_{kin} is the kinetic component of the fluid viscosity while μ_{coll} is the collisional component. The simplified equations for the components of the viscosity, omitting parameters that are set to 1 in our simulations, are as follows:

$$\mu_{\text{kin}} = \frac{\rho}{2} \left[\frac{\rho}{(\rho - 1 + e^{-\rho})} - 1 \right], \quad (5)$$

$$\mu_{\text{coll}} = \frac{1}{12} (\rho - 1 + e^{-\rho}), \quad (6)$$

where ρ is the average number of particles per collision cell. Since we use a density $\rho = 10$, the viscosity in our simulation units is 1.306.

C. Boundary conditions

At the macroscopic scale of organisms, there should be no slip at the interface between a fluid and a solid. This means that the fluid's tangent velocity to any surface at the interface should be zero—the so-called no-slip condition. We use two complementary methods from previous implementations of the model to ensure minimum slip, i.e., the virtual particle rule of Lamura and Gompper [17], and the random-reflect boundary condition [12,23], both of which are outlined below.

Lamura and Gompper [17,18] enforce no-slip boundary conditions in the collisional part of the model by including virtual “solid” particles in cells which partially overlap the solid. These virtual particles are included in the collisions among particles. The velocities of the virtual particles are

drawn from a Maxwell-Boltzmann distribution of mean zero and temperature $k_B T$. The mean of zero reduces slip while the temperature $k_B T$ causes the virtual particles to act as thermostats.

In the random-reflect boundary-condition particles that hit the solid get a new randomly chosen velocity. The new velocity is relative to the surface and consists of a tangential component v_t and normal component v_n , drawn from the following distributions [12,23]:

$$P(v_t) \propto e^{-\beta v_t^2}, \quad (7)$$

$$P(v_n) \propto v_n e^{-\beta v_n^2}. \quad (8)$$

Here, $\beta = \frac{m}{2k_B T}$. Since the new velocities are Maxwell-Boltzmann distributed with temperature $k_B T$ and a mean velocity tangential to the surface of zero, this method reduces slip and has the additional advantage that it makes solids act as thermostats. We prefer this method over the bounce back reflection used by Lamura and Gompper [17] in which particles reverse their velocity when they hit a solid. At small scales, a surface is not smooth and thus random reflection is a better approximation.

When particles move, they may collide with a solid. Because the particles keep moving after a collision, a series of collisions can occur within one time step Δt if there are multiple objects or if the shape of the object is complex. We therefore use the following iterative procedure.

For each particle, the time δt it has spent moving during this time step is set to 0. Then, as long as δt is smaller than the length of a time step Δt (Table I), the particle keeps moving. Its projected movement is calculated from its velocity vector \mathbf{v}_i as follows: $\mathbf{v}_i(\Delta t - \delta t)$. If this line intersects a solid, a collision occurs at the collision point \mathbf{x}_{coll} and δt is increased by the amount of time it took to move there. The particle is assigned a new random velocity following Eqs. (7) and (8). If δt is smaller than Δt , it keeps moving, starting from \mathbf{x}_{coll} and checking for collisions in the same manner.

D. Flow

The expected flow profile in an empty channel is known as Hagen-Poiseuille flow. This flow is characterized by a parabolic flow profile in a cross section of the channel, with the speed in the x direction on each point of the y axis given by

$$v_x(y) = \frac{4v_{\text{max}}(W-y)y}{W^2}, \quad (9)$$

where v_{max} is the maximum speed, in the center of the channel of width W .

To create flow we apply a constant force mg in the x direction to all fluid particles [21]. In an experiment this force would correspond to a pressure drop per unit length given by $\partial P / \partial x = -\rho mg$. We use a Galilean-invariant thermostat [12] to keep the system temperature constant. Due to the no-slip condition the channel walls exert a shear force, which increases with the flow speed and the viscosity μ . The system is stable when the gravitational force on the fluid is

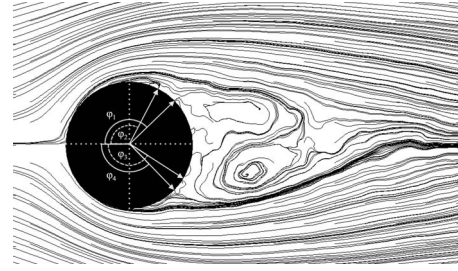


FIG. 2. The separation angle ϕ_i . The four lines are estimates of the minimum and maximum separation angle on each side of the object.

exactly balanced by this shear force. In this steady state the flow is laminar Hagen-Poiseuille flow, with the speed in the center of the channel v_{max} given by

$$v_{\text{max}} = \frac{\rho W^2 g}{8\mu}. \quad (10)$$

This method to create flow is different than that used by Lamura and Gompper [17,18], who imposed the Hagen-Poiseuille distribution [Eq. (9)] directly on particles in a “driving” section of their simulation. However, this causes a significant disruption of the flow: in the simulation area di-

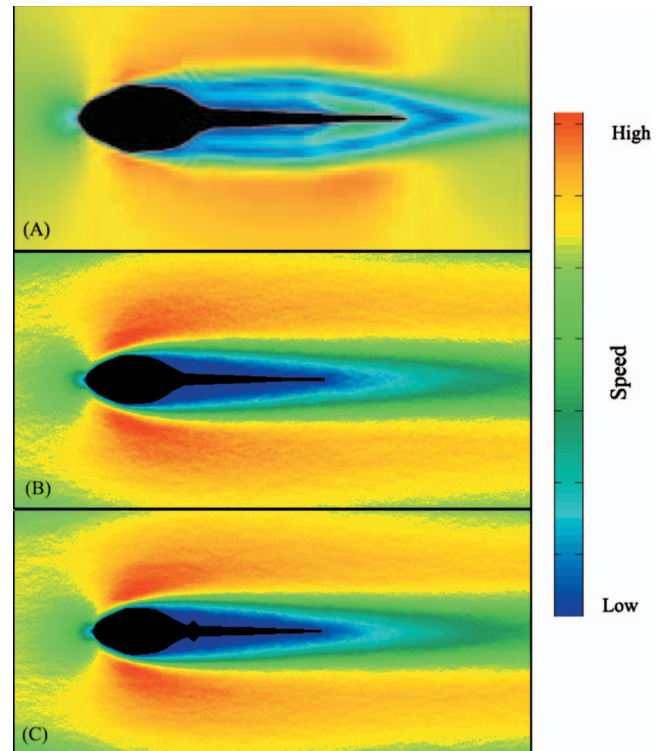


FIG. 3. (Color) Flow fields around a tadpole shape. (a) From Ref. [10], (b) in our model, and (c) in our model with added leglike protrusions. Color indicates flow speed, with high speed indicated by red and low speed by blue. Our simulations are at Reynolds numbers of approximately 105, based on the cross-channel size of the object. Figure (a) reproduced with permission of the Company of Biologists.

TABLE II. Drag coefficients for various shapes, with and without attached splitter or leglike protrusions. Reynolds numbers are shown both based on width as is common in physics (width) and on length as is common in biology. All Reynolds numbers discussed in this paper are width based. All simulations are two dimensional.

Shapes without and with splitter				
Shape	Re (Width)	Re (Length)	C_D	C_D with splitter
Square	80	80	1.8	1.45
Circle	115	115	1.22	1.05
Flat Plate	70	1.75	2.0	1.7

Fishlike shapes without and with legs				
Shape	Re (Width)	Re (Length)	C_D	C_D with legs
Tadpole	110	528	1.01	1.01
Straight fish	110	724	0.97	1.22
Undulated fish	110	724	1.9	N.A.

rectly adjacent to the driving section large vortices are formed along the channel walls, and the density of the fluid increases. Furthermore, the overall flow velocity in the channel does not become uniform, with significantly reduced flow speeds further away from the driving section due to channel friction. We therefore use gravity-driven flow.

If the system starts at rest, the time required to reach this steady state depends on the system size. This was approximately 50 000 time steps for the larger system sizes we examined. However, since we can estimate the final v_{\max} using Eq. (10), we can initialize the system with Hagen-Poiseuille flow of the appropriate speed using a Maxwell-Boltzmann distribution of temperature $k_B T$, with an average speed in the y direction of zero, and an average speed in the x direction according to Eq. (9). This means that for the empty channel the system does not need time to stabilize.

For a clear wake structure to develop behind a static object in the channel, the simulation must be run until it stabilizes. In that case the flow profile far away from the object is still parabolic, but due to the drag of the object it is slower

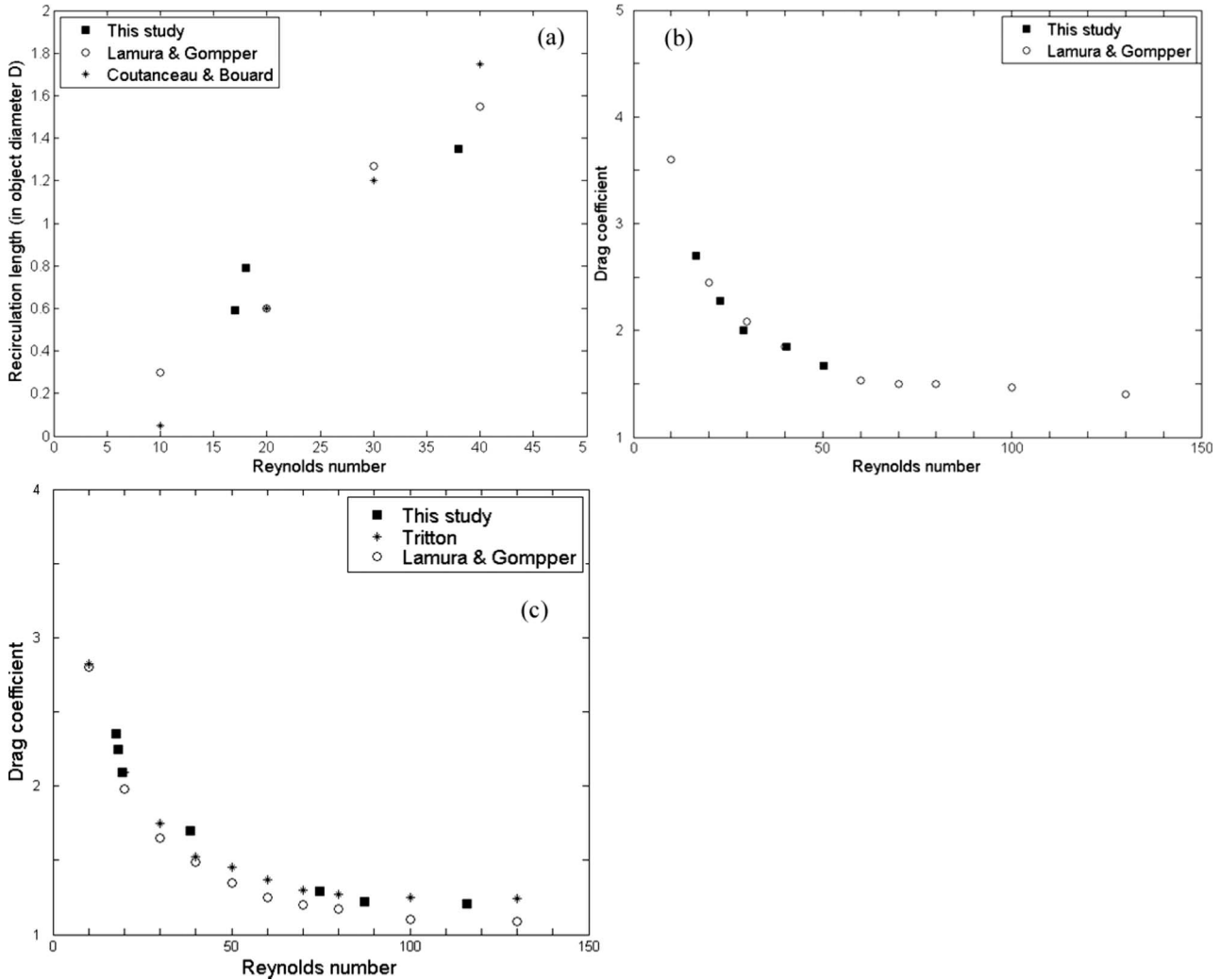


FIG. 4. Results of simulations for basic shapes. (a) The recirculation length for the circular cylinder as a function of the Reynolds number. Data from Ref. [18] (○), this study (■), and Ref. [27] (*). Note that steady recirculation only occurs at Reynolds numbers below 45. (b) The drag coefficient for the square cylinder as a function of the Reynolds number. Data from Ref. [18] (○), and this study (■). (c) The drag coefficient for the circular cylinder as a function of the Reynolds number. Data from Ref. [28] (*), Ref. [18] (○), and this study (■).

than estimated by Eq. (10). Tests showed that at the Reynolds numbers we examined the speed is lower by about 60% if an object is present, therefore we initialize the system with Hagen-Poiseuille flow of v_{\max} 60% slower than expected for the empty channel. Such an initialization of the flow field reduces the time required to reach the steady state by approximately 50% compared to starting the simulation from a resting fluid.

E. Measurements

The recirculation length in the regime of steady recirculation [17] is measured as the length of the area of recirculation in the wake of the object. It is defined as the distance from the rear end of the cylinder to the end of the wake. We define the end of the wake as the rearmost point on the central axis where the average flow in the x direction is zero. We express the recirculation length in terms of the object diameter D .

The drag coefficient C_D [17] is defined as

$$C_D = \frac{2F_x}{\rho_m v^2 D}, \quad (11)$$

where F_x is the force on the object in the direction of flow (in $ma_0\delta t^{-2}$) caused by the change of momenta of the colliding particles, ρ_m is the density of the fluid (in ma_0^{-2}) which equals the density of particles ρ due to our choice of parameters (Table I), v (in $a_0\delta t^{-1}$) is the flow speed in the center of the channel far away from the object, and D is the cross-channel width of the object measured in a_0 .

The angle of separation is the angle between the central x axis and the separation point. A separation point is defined as a point close to the surface where the flow velocity tangential to the surface is zero (of course everywhere *on* the surface the average tangential velocity is zero because of the boundary conditions). An object in low-Reynolds flow always has separation points at angles 0 and 180, but at sufficiently high Reynolds numbers two new separation points occur toward the rear of the object. To measure the separation angle of these two new separation points, we draw a line from the center of the object to the separation point, and measure the angle ϕ between that line and the central x axis (Fig. 2). As can be seen from Fig. 2, the precise angle of separation is difficult to determine because the flow is stochastic. We therefore estimate a minimum and maximum separation angle at each side of the object by hand, and use the average of these four values.

All programs were implemented in C++ and simulations were run on single Intel Core2 Duo PCs. Data analysis and visualization were done with MATLAB® [24]. The tadpole form was traced from a figure of a cross section of a bullfrog tadpole (*Rana catesbeiana*) by Liu *et al.* [10]. The fish shape was traced from a figure of a cross section of a mullet (*Chelon labrosus*) by Müller *et al.* [25]. Simulation time for the largest simulation, namely of a fish shape at Reynolds number 110, took approximately 10 days.

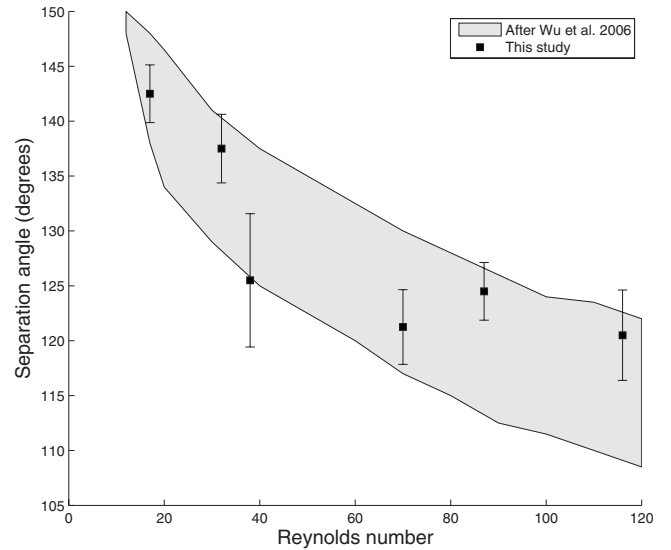


FIG. 5. The separation angle for the circular cylinder as a function of the Reynolds number. Data from an overview of experimental data from Ref. [29] (gray area) and mean values \pm standard error of this study (■).

III. RESULTS

When we compare the flow field of the tadpole in our model to that in the numerical model by Liu *et al.* [10,26], it appears to be qualitatively similar as regards the area of low flow speed around the tail [Figs. 3(a) and 3(b)]. In further agreement with their results, the addition of leglike extrusions to it changes neither the flow field nor the drag coefficient [Fig. 3(c)]. This confirms the conclusion of Liu *et al.* [10] that the location of leg growth in tadpoles is neutral in terms of drag.

In contrast, when we add such extrusions to a fish shape, the drag coefficient increases by 25%, from 0.97 to 1.22. The drag coefficient is also higher for an S-shaped fish than for a straight one with an increase of 95%, from 0.97 to 1.9, (Table II).

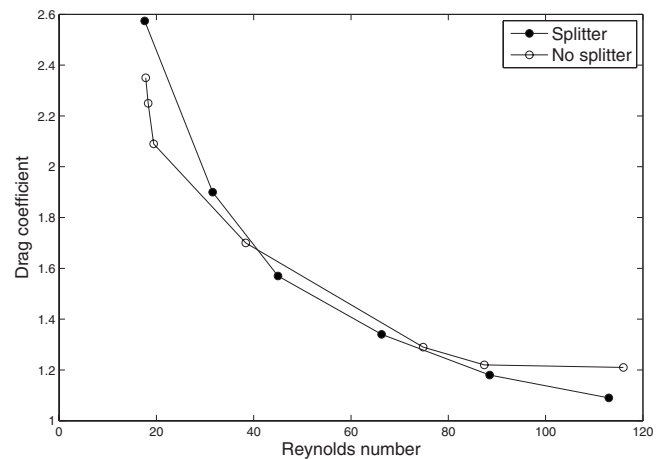


FIG. 6. The drag coefficient of the circular cylinder as a function of the Reynolds number. Plotted values are for the cylinder with (●) and without (○) trailing splitter plate.

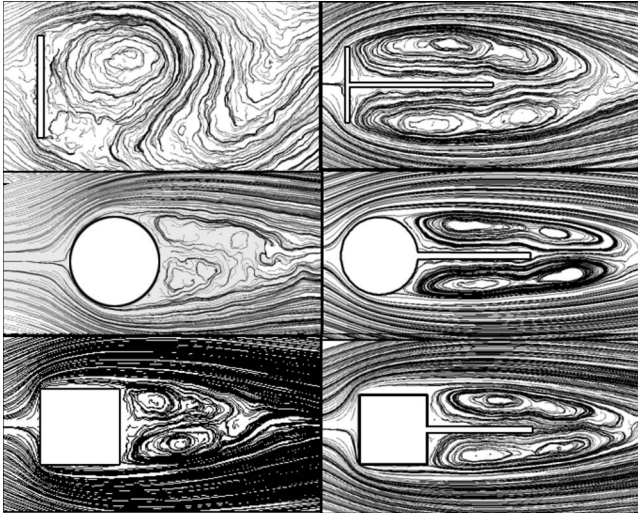


FIG. 7. Streamlines for flat plate, circle, and square with and without splitter plate attached. The Reynolds number is approximately 80. Note that the flat plate and splitter plates are thicker than the mesh cell size a_0 . The cross-channel diameter of the objects is the same in all cases.

The shape of a tadpole and its drag coefficient resemble those of a circular cylinder with an attached splitter plate (Table II). As regards the recirculation length and drag coefficient of the circular cylinder and the drag coefficient of the square cylinder [Fig. 4], our results resemble those of the model by Lamura and Gompper [17] as well as empirical data [27,28]. Furthermore, the angles of separation of flow (Fig. 5) fall within the range of empirical data from Wu *et al.* [29].

We test in our model the hydrodynamics of attached splitter plates by measuring the drag of a circular cylinder over a range of Reynolds numbers, both with and without an attached splitter plate. Due to the splitter plate, the drag coefficient of the cylinder becomes higher at low-Reynolds numbers due to additional friction drag (Fig. 6). At higher Reynolds numbers (Fig. 6) however, the splitter plate stabilizes the wake and delays the onset of vortex shedding (Fig. 7), which lowers the drag. We find that at these Reynolds numbers splitter plates also reduce the drag of a square cylinder and flat plate (Table II).

IV. DISCUSSION

The results of our simulations show that at intermediate Reynolds numbers the multiparticle collision dynamics model is suitable to investigate the hydrodynamics of fishlike shapes. Our quantitative measurements agree with data of empirical and model studies. Thus, the model is robust against adjustments of the boundary conditions and the method to drive the flow. Further, flow around shapes of fish and tadpoles qualitatively resembles that of numerical investigations [10].

TABLE III. Critical Reynolds numbers for the onset of flow phenomena for circular cylinder (2D) [29–31] and sphere (3D) [31,32].

Flow phenomenon	Re 2D	Re 3D
Recirculation	10	25
Vortex shedding	45	280
Turbulence	1.2×10^5	4.7×10^5

As to the measurements of the recirculation length [Fig. 4(a)], these tend to be too low at higher Reynolds numbers both in our results and in those of Lamura and Gompper [17,18]. This arises probably because the wake sometimes deviates from the central axis along which it is measured, and this deviation will cause an underestimation. The size of this error is larger if the wake is longer, and therefore it is larger at high Reynolds numbers. This is due to the considerable stochasticity of flow. Another consequence of this stochasticity is that to maximally reveal patterns of flow, drag *et cetera*, data had to be averaged over an interval of many time steps (to the order of hundreds). This interval was still much shorter than the cycle of the phenomena we studied. Note that this averaging is common practice in studies of multiparticle collision dynamics.

It is likely that the width-to-length ratio and blockage ratio of the channel have an effect on flow and drag. We did not study this however, because our future work will concern flow that is not confined between walls.

In the future we intend to study the hydrodynamics of the locomotion of fish. Fish swim at Reynolds numbers between 10^3 and 10^5 as measured by biologists, which is much higher than those used in this study. However, the following factors will help us to work in the model in the correct range of Reynolds numbers. First, the Re numbers measured by biologists are based on the length of the fish, those by physicists on its thickness. This reduces the Re number to about one-fifth. Second, we may study these undulating fish at somewhat lower Re numbers because real fish swim in three dimensions (3D), whereas our model is a representation in two dimensions (2D). Two dimensions restrict the degrees of freedom of movement and hence, all phenomena—such as recirculation, vortex shedding, and turbulence—occur at half (or less) the Reynolds number of that in 3D (Table III). Thus, wakes of fish in our model may develop sooner too.

We conclude from our results that the multiparticle collision dynamics method is suitable for the study of flow around stiff fishlike shapes. We will therefore proceed to investigate its suitability for the study of fish that move.

ACKNOWLEDGMENTS

H.H. and C.K.H. were financed by Grant No. 012682-STARFLAG from the STREP-program “Starflag” in the 6th European framework. J.T.P. thanks the Netherlands Organization for Scientific Research (NWO) for financial support.

- [1] M. Breuer, J. Bernsdorf, T. Zeiser, and F. Durst, *Int. J. Heat Fluid Flow* **21**, 186 (2000).
- [2] E. Falck, J. M. Lahtinen, I. Vattulainen, and T. Ala-Nissila, *Eur. Phys. J. E* **13**, 267 (2004).
- [3] M. Ripoll, K. Mussawisade, R. G. Winkler, and G. Gompper, *Europhys. Lett.* **68**, 106 (2004).
- [4] T. Sakai, Y. Chen, and H. Ohashi, *Comput. Phys. Commun.* **129**, 75 (2000).
- [5] H. Noguchi and G. Gompper, *Phys. Rev. E* **73**, 021903 (2006).
- [6] A. Malevanets and R. Kapral, *Europhys. Lett.* **44**, 552 (1998).
- [7] A. Malevanets and R. Kapral, *J. Chem. Phys.* **112**, 7260 (2000).
- [8] J. D. Eldredge, *J. Comput. Phys.* **221**, 626 (2007).
- [9] S. D. Kelly and R. M. Murray, *Int. J. Robust Nonlinear Control* **10**, 217 (2000).
- [10] H. Liu, R. J. Wassersug, and K. Kawachi, *J. Exp. Biol.* **199**, 1245 (1996).
- [11] H. Noguchi and G. Gompper, *J. Phys.: Condens. Matter* **17**, S3439 (2005).
- [12] J. T. Padding and A. A. Louis, *Phys. Rev. E* **74**, 031402 (2006).
- [13] N. Watari, M. Makino, N. Kikuchi, R. G. Larson, and M. Doi, *J. Chem. Phys.* **126**, 094902 (2007).
- [14] N. Kikuchi, C. M. Pooley, J. F. Ryder, and J. Yeomans, *J. Chem. Phys.* **119**, 6388 (2003).
- [15] J. J. Videler, *Fish Swimming* (Chapman and Hall, London, 1993).
- [16] U. K. Müller, E. J. Stamhuis, and J. J. Videler, *J. Exp. Biol.* **203**, 193 (2000).
- [17] A. Lamura, G. Gompper, T. Ihle, and D. M. Kroll, *Europhys. Lett.* **56**, 319 (2001).
- [18] A. Lamura and G. Gompper, *Eur. Phys. J. E* **9**, 477 (2002).
- [19] H. Liu, R. Wassersug, and K. Kawachi, *J. Exp. Biol.* **200**, 2807 (1997).
- [20] K. Kwon and H. Choi, *Phys. Fluids* **8**, 479 (1996).
- [21] E. Allahyarov and G. Gompper, *Phys. Rev. E* **66**, 036702 (2002).
- [22] T. Ihle and D. M. Kroll, *Phys. Rev. E* **63**, 020201(R) (2001).
- [23] Y. Inoue, Y. Chen, and H. Ohashi, *Comput. Phys. Commun.* **142**, 114 (2001).
- [24] The MathWorks, *MATLAB r2006a*.
- [25] U. K. Müller, B. L. E. van den Heuvel, E. J. Stamhuis, and J. J. Videler, *J. Exp. Biol.* **200**, 2893 (1997).
- [26] H. Liu and K. Kawachi, *J. Comput. Phys.* **155**, 223 (1999).
- [27] M. Coutanceau and R. Bouard, *J. Fluid Mech.* **79**, 231 (1977).
- [28] D. J. Tritton, *J. Fluid Mech.* **6**, 547 (1959).
- [29] M. H. Wu, C. Y. Wen, R. H. O. R. Yen, M. C. Weng, and A. N. B. Wang, *J. Fluid Mech.* **515**, 233 (2004).
- [30] P. Paranthoën, L. W. B. Browne, S. Le Masson, F. Dumouchel, and J. C. Lecordier, *Eur. J. Mech. B/Fluids* **18**, 659 (1999).
- [31] S. F. Hoerner, *Fluid-Dynamic Drag* (Hoerner Fluid Dynamics, Bakersfield, CA, 1968).
- [32] S. Taneda, *J. Phys. Soc. Jpn.* **11**, 1104 (1956).